FLOW MALDISTRIBUTION IN THE ANODE OF A POLYMER ELECTROLYTE MEMBRANE WATER ELECTROLYSIS CELL EMPLOYING INTERDIGITATED CHANNELS

Anders Christian Olesen *and **Søren Knudsen Kær**
Aalborg University
Department of Energy Technology
9220 Aaborg East
Denmark

ABSTRACT

In this work a macroscopic, steady-state, three-dimensional, computational fluid dynamics model of the anode of a high-pressure polymer electrolyte membrane electrolysis cell (PEMEC) is presented. The developed model is used for studying the effect of employing an interdigitated, planar-circular cell design on the distribution of water in the anode. In the electrolysis of water using PEMEC the anode is fed by demineralized water. Throughout the anode, oxygen is produced and a two-phase flow develops. Interdigitated channels assist in avoiding that gaseous oxygen obstructs the transport of liquid water towards the catalytic layer of the electrode. As opposed to the more common serpentine and parallel channels, interdigitated channels force liquid water through the porous gas diffusion layer (GDL) of the electrode. This improves the supply of water, however it increases pressure losses. While interdigitated channels have been examined for planar-square cells in detail, less is known for planar-circular cells. To examine the extent of flow maldistribution, a base case is defined and a parameter variation is conducted relative to it. In the study, the following parameters are examined: water stoichiometry, temperature, GDL permeability and thickness. In conclusion, it is found that the interdigitated flow field results in an uneven distribution across the cell and that the extent depends strongly on the permeability and weaker on the remaining parameters.

Keywords: Flow maldistribution, PEMEC, Electrolysis, Modeling

NOMENCLATURE

U	Velocity	[m/s]
K	Permeability	[m]
p	Pressure	[Pa]
N	Number of channels	[m]
A	Area	[m^2]
S	Source term	[kg / (m^3 s)]
L	Channel length	[m]
T	Temperature	[K]
J	Current density	[A/cm^2]
$\dot{m}$	Mass flow	[kg/s]
ε	Volume porosity	[-]
ρ	Density	[kg/m^3]
σ	Standard deviation	[-]
F	Faradays constant	[C/mol]
L_T	Gas diffusion layer thickness	[m]
λ	Stoichiometric factor	[-]
μ	Mean	[-]
μ	Dynamic viscosity	[Pa s]
$\mathbf{M}$	Interfacial forces	[kg/(m^{3}s)]
$\mathbf{n}$	Normal vector	[-]
r_p	Fiber radius	[m]
ε_p	Percolation threshold	[m]
n_r	Moles of reactant required	[mol]
n_s	Moles of reactant supplied	[mol]
α	Directional dependent parameter	[-]
M_W	Molecular weight	[kg/kmol]
$\mathbf{i}$	Identity matrix	[-]

*Corresponding author: Phone: +45 2139 9153 E-mail:aco@et.aau.dk

INTRODUCTION

The production of hydrogen through water electrolysis has received growing attention in recent years [2, 1]. This interest has partially been sparked by the growing demand for sustainable produced hydrogen in fuel cell applications and partially by the demand for energy storage during peak production periods especially associated with the increasing use of sustainable power sources like wind turbines and solar power [4, 6, 3]. As a technology water electrolysis has been commercially available for nearly a century. These systems have typically been alkaline based, very bulky, inefficient and suffered from poor dynamic response to load changes. With the recent developments of polymer electrolyte membrane electrolysis cells (HP PEMEC), a technology has been developed that offers significant higher energy densities, current densities, efficiency as well as a good dynamic response. [1]

In the electrolysis of water using PEMEC the overall reaction is split into two half-cell reactions occuring at the anode and cathode, respectively:

$$2H_2O \rightarrow 4H^+ + 4e^- + O_2 \qquad (1)$$

$$2H^+ + 2e^- \rightarrow H_2 \qquad (2)$$
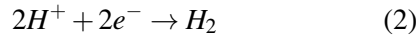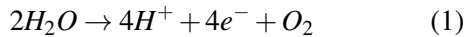
While electricity is supplied to the PEMEC, the anode is fed with demineralized water. Throughout the anode, oxygen is produced and a two-phase gas-liquid flow develops. Similarly in the cathode, hydrogen is produced along the channel length. Since water can permeate the polymer membrane, two-phase gas-liquid flow can also occur at the cathode. Although PEMEC are competitive on many levels, durability and lifetime still need to be improved. One way is by optimizing the flow distribution across the cell. Because the incoming liquid water both serves as a fuel and coolant, an even distribution not only ensures good mass transport characteristics, it also allows for an even heat removal. If either of these issues cannot be ensured, the risk of hotspots and catalyst degradation increases. As opposed to PEM fuel cells (PEMFC), which are typically operated at low pressures (e.g. 1 bar), it is an advantage to operate PEMEC at elevated pressures of up to 200 bars and thereby decreasing the need for subsequent compression of the hydrogen to store it.


(a) Parallel   (b) Serpentine

(c) Interdigitated
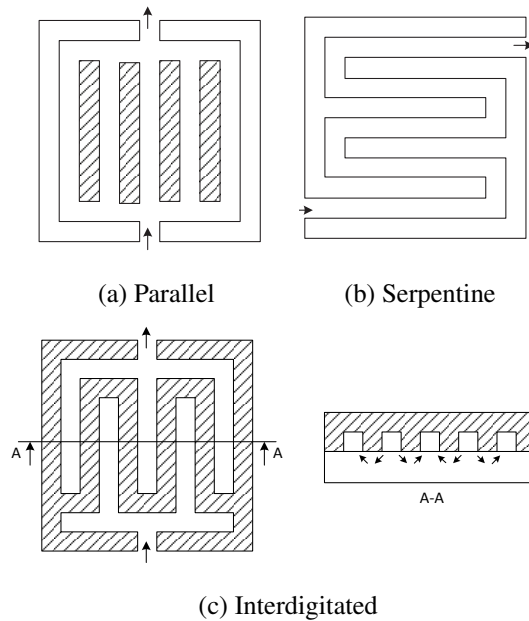
Figure 1: Three archetype channel configurations for square-planar cells

To improve mechanical stability at elevated pressuresm circular-planar cells are used instead of square-planar cells. Evidently, this difference in outer geometry affects the channel design. Another difference that affects channel design is the difference in two-phase morphology. In PEMFC the two-phase flow consists of a continuous gaseous phase and a dispersed liquid water droplets phase. However, in PEMEC this is only true for the cathode; in the anode the continuous phase consists of liquid water and dispersed oxygen bubbles.

For square-planar cells three archetype channel configurations are traditionally considered [5], although more types exist [10]. These are parallel, serpentine and interdigitated channels. A schematic drawing of each type is shown in Figure 1. While parallel and serpentine channels distribute reactants over a porous gas diffusion layer (GDL), through which species mainly diffuse, interdigitated channels forces convective flow through the GDL. Interdigitated flow fields therefore offer better mass transport, whereas parallel and serpentine offer a significant lower pressure loss. For systems subject to two-phase flow, parallel channels suffer from a high extent of flow maldistribution, since a single channel might become blocked by a gas bubble or liquid droplet. To circumvent this blocking or at least reduce it, combinations of parallel and serpen-

tine channels are often used. In interdigitated flow fields the reactant phase in the two-phase flow is much less prone to becoming blocked, since the reactant phase is convectively transported through the GDL. Nevertheless, it should be noted that the exact characteristics of each archetype depends on channel length, channel height, channel width and number of channels.

In the literature, various experimental and modeling studies have been conducted for square-planar cells in PEMFC comparing interdigitated flow fields with parallel or serpentine fields. Among others, Wang and Liu 2004 [8], Wang et al. [9] and Berning et al. 2014 [7] have demonstrated the improved reactant mass transport in the presence of two-phase gas-liquid flow by switching to an interdigitated flow field. Furthermore, the study by Berning et al. 2014 [7] underlined that an improved waste heat removal could be seen.

For PEMEC the available number of publications is scarcer. A few studies have investigated the effect of two-phase gas-liquid flow in the anode using parallel and serpentine flow fields in PEMEC at low pressures. Ito et al. 2010 [11] found in their experimental study that these flow fields are sensitive to the two-phase flow regime. At high current densities when a high amount of oxygen is produced slug or annular two-phase flow develops and obstructs the liquid reactant phase flow towards the catalyst layer. In the numerical modeling study by Nie and Chen 2010 [12] it was further shown that a high extent of flow maldistribution could occur. Even reversed flow was observed in some channels.

Although the use of an interdigitated, square-planar flow field in PEMFC has been shown to offer particular benefits in avoiding mass transport limitations induced by two-phase gas-liquid flow, no studies are available for interdigitated, circular-planar flow fields of PEMEC. In particular, the benefit of interdigitated flow fields for the anode is unknown. The main objective of this work is therefore the investigation of flow maldistribution in an interdigitated PEMEC anode flow field. As a first attempt, two-phase gas-liquid flow phenomena are disregarded, and only single-phase flow is considered. This is done in order to get a clear effect of the circular-planar cell design, rather than a mixed effect from both.

In the following, a parametric study of a macro-scopic, steady-state, three-dimensional, single phase model is presented. The model accounts for mass and momentum transport in channels and the porous GDL. Initially, a short description of the geometry, mathematical model, numerical solver and data treatment will be given, followed by a grid independency study. Then, results from a base case and parametric study are analyzed and discussed.

METHODOLOGY

In this work the interdigitated, circular-planar flow field shown in Figure 2 is used. It consists of one inlet, one outlet, an interdigitated channel structure and a porous medium. There are 8 incoming and 9 outgoing channels in the interdigitated channel structure. Each channel has a width of 1 mm and height of 0.5 mm. The inlet manifold has a height of 1 mm and width of 5 mm. The diameter of the circular GDL is 10 cm.
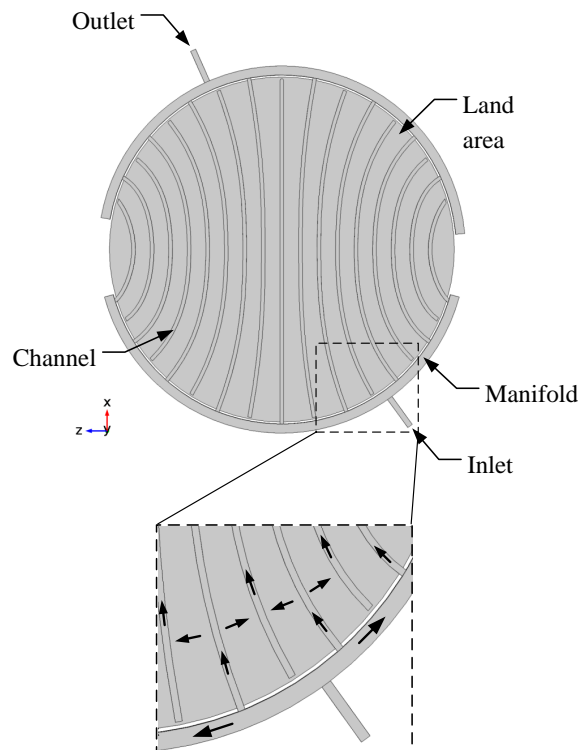

Figure 2: Interdigitated flow field geometry

The channels are fairly thin compared to the land width, however this is to avoid that the porous medium intrudes into the channels. Moreover, the channels are curved to minimize the difference in length between them; however this comes at the expense of an uneven land width.

The zoomed area in Figure 2 highlights the flow direction in the geometry. Flow from the inlet, the liquid is distributed in the inlet manifold and hereafter in the inlet channels. Then, the flow is forced underneath, through the GDL, and out through each outlet channel. The flow from the outlet channels then merge in the manifold and flow out of the geometry.

Mathematical Equations

To obtain the velocity and pressure field distribution inside channels and porous media the macroscopic, volume-averaged, steady-state continuity and momentum conservation equations are solved in eqn. 3 and 4, respectively:

$$\nabla \cdot (\varepsilon \rho \mathbf{U}) = \varepsilon S \tag{3}$$

$$\nabla \cdot (\varepsilon \rho \mathbf{U}\mathbf{U} - \varepsilon \tau) = \varepsilon (\mathbf{S} - \nabla p) + \varepsilon \rho \mathbf{g} + \varepsilon \mathbf{M} \tag{4}$$

$$\tau = \mu \left(\nabla \mathbf{U} + (\nabla \mathbf{U})^T - \frac{2}{3} (\nabla \mathbf{U}) \mathbf{I} \right) \tag{5}$$

Here $\mathbf{U}$ is the true velocity, ρ is density, ε is the volume porosity, which is 1 outside the GDL, τ is the stress tensor, $\mathbf{I}$ is the identity matrix, $\mathbf{g}$ is the gravity vector, S is a mass source, p is pressure, $\mathbf{S}$ is a momentum source term, μ is the dynamic viscosity and $\mathbf{M}$ covers the interfacial forces acting on phase in the porus medium, else it is zero.

For laminar flow in porous media the interfacial force is given by Darcy's law:

$$\mathbf{M} = \frac{\mu \varepsilon}{K} \mathbf{U} \tag{6}$$

Here K is the viscous permeability. The viscous permeability of a fibrous porous medium, which is typically used, can be estimated via the following empirical correlations as a function of porosity [15]:

$$K = \frac{\varepsilon}{8 (\ln \varepsilon)^2} \frac{(\varepsilon - \varepsilon_p)^{\alpha+2} r_f^2}{(1 - \varepsilon_p)^{\alpha} ((\alpha+1)\varepsilon - \varepsilon_p)^2} \tag{7}$$

Here ε_p is the percolation threshold porosity, which for two-dimensional fibrous structures is 0.11, r_f is the carbon fiber radius and α is a directional dependent parameter, which in the through-plane and in-plane direction is 0.521 and 0.785, respectively.

The framework for modeling macroscopic single-phase flow in porous media was originally developed by Slattery [14] and Whitaker [13], and later extended by numerous authors. For a general introduction to the topic of macroscopic modeling of porous media and the application of volume averaging, interested readers are referred to Jakobsen [16].

Boundary condition

The inlet mass flow of liquid water is calculated as follows:

$$\dot{m}_{in} = \frac{M_w \lambda j A_c}{2F} \tag{8}$$

Here M_w is the molecular weight, λ is the stoichiometric factor, j is current density, A_c is the cross-sectional area and F is Faradays constant.

In the context of fuel cell and electrolysis modeling the stoichiometric factor λ is defined as the number of moles of reactant supplied n_s relative to the number of moles required for a stoichiometric reaction n_r:

$$\lambda = \frac{n_s}{n_r} \tag{9}$$

Thus, a stoichiometric factor of 1 corresponds to the exact amount needed for a given current density, whereas a stoichiometric factor of 5 corresponds to 5 times the required amount for a given current density supplied.

Numerical Solver

The presented mathematical model was solved using the commercial software, COMSOL Multiphysics. In this software the partial differential equations are solved using the finite element approach. For laminar flow the default discretization scheme is the so-called P1+P1, where both the pressure and velocity are discretized using linear elements. The resulting non-linear algebraic matrix systems were solved using a coupled, multigrid solver.

Data Treatment

To be able to evaluate the extent of mass flow maldistribution in a systematic fashion a channel mass flow standard deviation is defined as follows:

$$\sigma = \sqrt{\frac{1}{N}\sum_{i=1}^{N}\left(\frac{\dot{m}_i}{L_i}-\mu\right)^2} \qquad (10)$$

$$\mu = \frac{1}{N}\sum_{i=1}^{N}\frac{\dot{m}_i}{L_i} \qquad (11)$$

Here σ is the channel mass flow standard deviation, μ is the average channel mass flow, N is the number of channels, $\dot{m}_i$ is the mass flow rate of each channel, and L is the channel length. The reason why the mass flow is devided by channel length is to account for the difference in channel length, and thus the difference in surface area and the need for water and cooling. The channel mass flow is calculated by integrating over the cross-sectional area of the channel outlet:

$$\dot{m}_i = \int_{A_i}\rho\mathbf{U}\cdot\mathbf{n}dA \qquad (12)$$

Here $\mathbf{n}$ is the normal vector of the cross-sectional area. The advantage of defining a channel mass flow standard deviation is the quantification of the flow maldistribution. However, to enable a direct comparion between the individual simulation cases in the parameter variation, the standard deviation needs to be normalised by the mean channel mass flow.

RESULTS AND DISCUSSION

In the parameter variation three different parameters are varied. In order to minimize the test matrix a base case reflecting nominal operation conditions is defined. From this point each parameter is then varied. The values of the base case are shown in Table 1.

Parameter	Symbol	Value	Unit
Temperature	T	343	K
Permeability	K	$1.0\cdot10^{-11}$	m^2
Porosity	ε	0.7	-
GDL thickness	L_T	200	μm
Stoichiometry	λ	100	-
Current density	J	1.0	A/cm^2

Table 1: Base case modeling properties

Before commencing with the results from the base case and parameter variation, a grid independency study is presented.

Grid Independency

The mesh required for the presented interdigitated geometry has to resolve large differences in length scales across the flow field; hence the number of cells is bound to be in the order of millions.
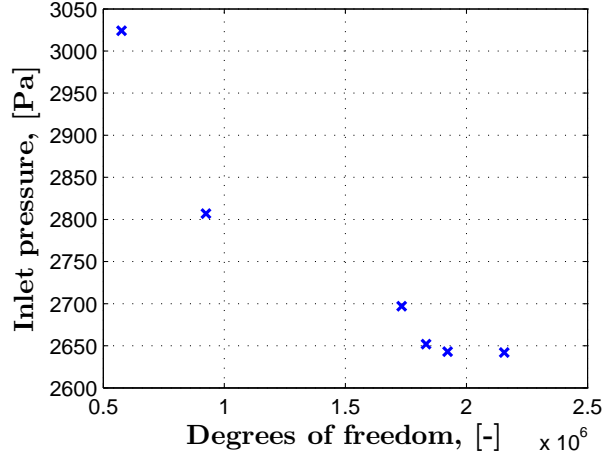

Figure 3: Grid independency study at 298 K

A grid independency study is carried out to ensure that only the minimum required number of cells, which guarantees a grid independent solution, is solved. In this study, the back pressure is monitored as the number of cells is gradually increased towards the maximum number of degrees of freedom that the computer can handle. As shown in Figure 3, a stable solution is reached around 2 million degrees of freedom. Thus, all simulation results presented in the following where obtained using a grid consisting of 1.95 million cells.

Base Case

To quantify the extent of flow maldistribution between channels, the obtained results from the base case are depicted in two ways: 2D contour plots in Figure 4 and bar plots in Figure 5. While 2D contour plots depict the velocity and pressure fields, the bar plots show the mass flow rate out of the channels with and without channel length normalization.

The velocity distribution within the GDL depicted in Figure 4a can be used as an indicator of how well cooling and mass transport occurs. The higher the velocity, the better the effect is, and vice versa. The highest velocities are found near the outer interdigitated channels. Velocities then appear to gradually

(a) Velocity distribution in the gas diffusion layer $(y/t_{GDL} = 0.5)$

(b) Velocity distribution in channels and manifold $(y/t_{channel} = 0.5)$

(c) Surface pressure distribution
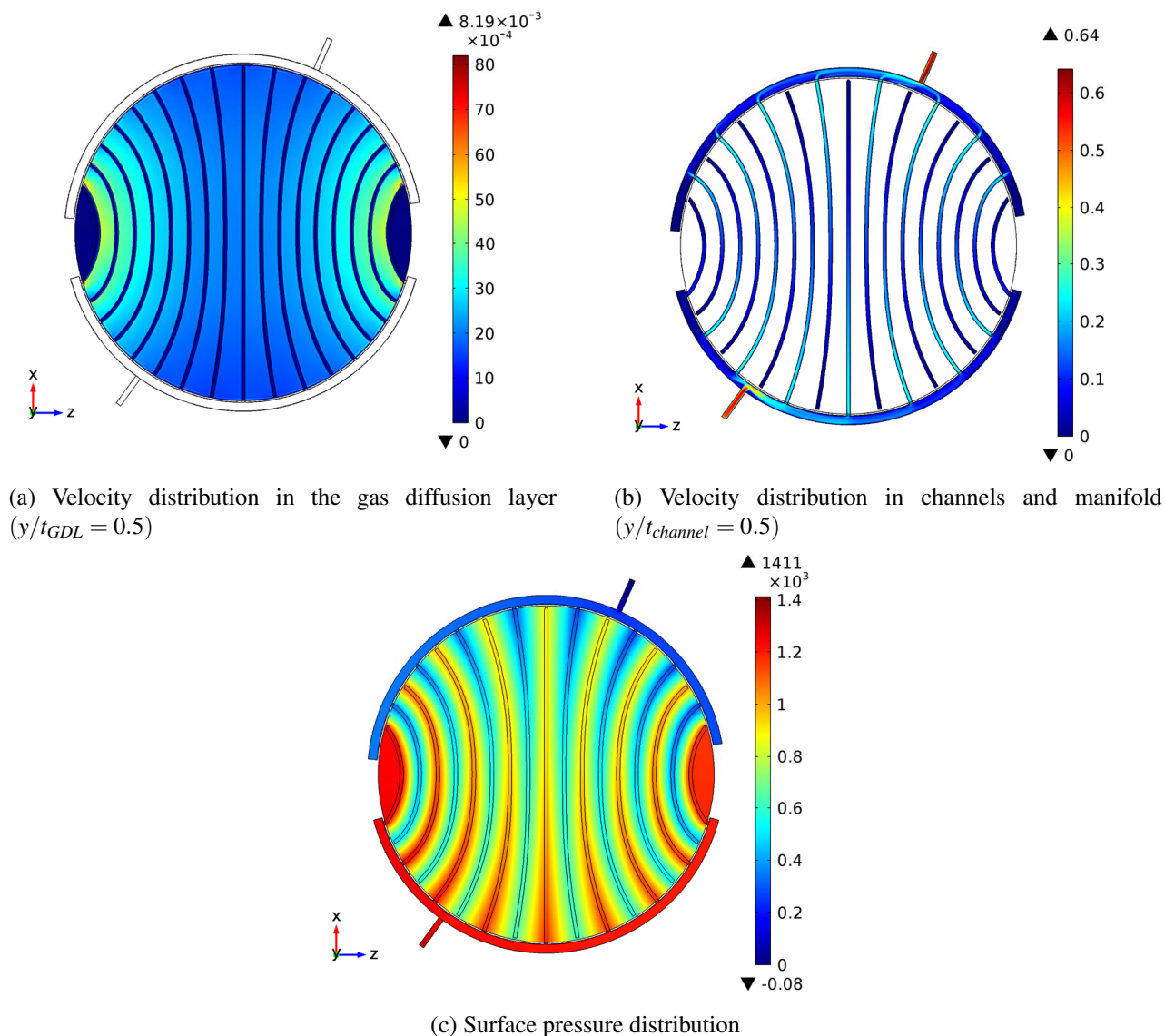
Figure 4: Crosssectional contour plots

decrease from the outer channels and towards the center of the plate. Two low velocity zones can further be identified. These occur because fluid flow is not forced through the GDL here.

In Figure 4b the velocity distribution within the interdigitated channels and manifold can be seen. The velocity distribution reveals large differences throughout the geometry. At the inlet, a high velocity jet is formed, which creates a high dynamic pressure zone as seen in Figure 4c. Similarly high velocities can be observed into and out of each interdigitated channel due to a reduced cross sectional channel area. Interestingly, these large velocity differences between each channel and the manifold make it possible to clearly observe how the fluid flow out

of each channel mixes into the manifold flow.

From the pressure distribution in Figure 4c it should be noted that the pressure loss through the system is 1411 Pa under the prescribed conditions. It is clearly visible that the majority of the pressure loss originates from the convective flow through the GDL. However, some extent of uneven pressure distribution within the manifold is visible. It can further be observed that the land area width is larger for channels near the center of the plate. Hence, pressure losses are bound to be higher here, which in turn corresponds to a lower mass flow

When comparing the mass flows through each interdigitated channel in Figure 5a, it appears that a fairly even distribution is obtained with the excep-
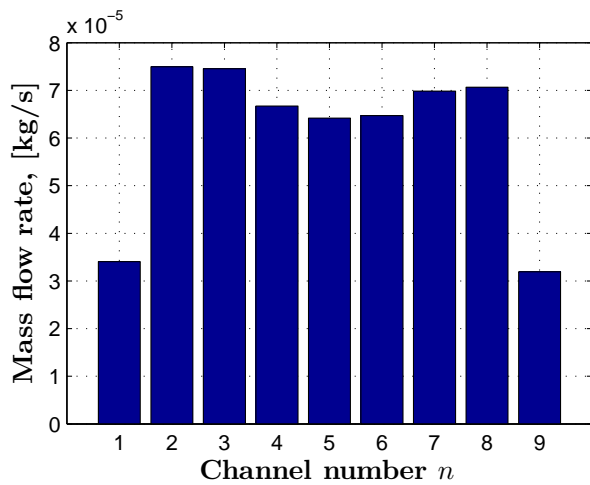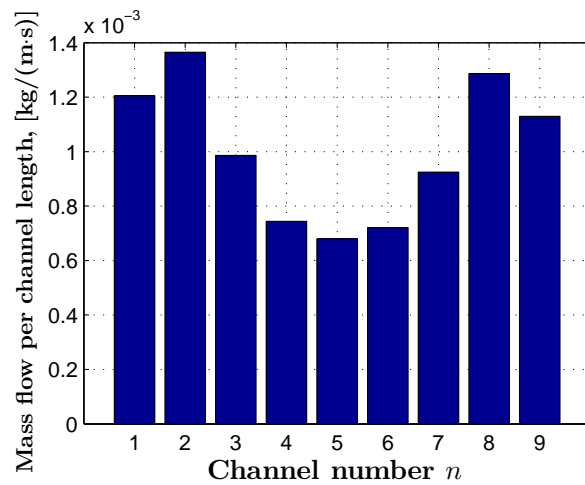
Figure 5: Channel mass flow with (a) and without (b) channel lenght correction, respectively.

tion of channel 1 and 9. Meanwhile, when accounting for the difference in channel length, this picture changes dramatically, as can be seen from Figure 5b. It now becomes evident that especially channel 4 to 6 suffer from a lower mass flow rate relative to the cross-sectional area they need to supply with water and coolant. For these channels the local water stoichiometry would be roughly half compared to the outer channels. The observation that the mass transport gradually improves towards the outer channels is in good agreement with the velocity distribution in the GDL shown in Figure 4a. Moreover, it further emphasizes that merely studying mass flows rather than mass flows per channel length does not reveal the extent of flow maldistribution.

A further comparison between the individual channels reveals a non-symmetric mass flow distribution. This indicates that the position of the inlet and outlet to some extent is significant. If the inlet and outlet where positioned in the middle, a symmetric distribution would be expected.

Parameter Variation

The obtained results from each parameter variation are depicted as x-y plots in Figure 6. In each subfigure, the standard deviation is shown on the y-axis and the parameter in question on the x-axis.
It can be observed in Figure 6a that the normalized standard deviation increases as a function water stoichiometry. This means that the extent of flow maldistribution increases proportionally to the water stoi-

chiometry. Hence, when higher flows are needed, in order to cool the cell, an inherent more non-uniform cooling is enforced.

From Figure 6b, it can be observed that the normalized standard deviation shows a strong dependence on viscous permeability. As the permeability gradually decreases, the normalized standard deviation rapidly follows. However, ones the permeability reaches a value around $1.0 \cdot 10^{-11}$ m^2, the change in the normalized standard deviation begins to decrease significantly. In fact, it appears that the standard deviation asymptotically approaches a constant value. The identified threshold seems to indicate a transition towards a porous medium dominated maldistribution. Above this point, the flow between the channels is important, whereas below primarily the flow through the porous medium is.

Decreasing the permeability is equivalent to increasing the flow resistance; this can likewise be achieved by decreasing the GDL thickness while keeping the permeability constant. However, as seen from Figure 6c, the change in normalized standard deviation only shows a weak dependence on GDL thickness compared to the viscous permeability. Evidently, the possible benefit is rather limited in comparison.

In Figure 6d, a weak temperature dependence of the normalized standard deviation can be observed. The temperature affects fluid density and viscosity. The higher the temperature is, the lower both become. Since the viscous shear stress in the channel and porous medium both linearly dependent on viscos-
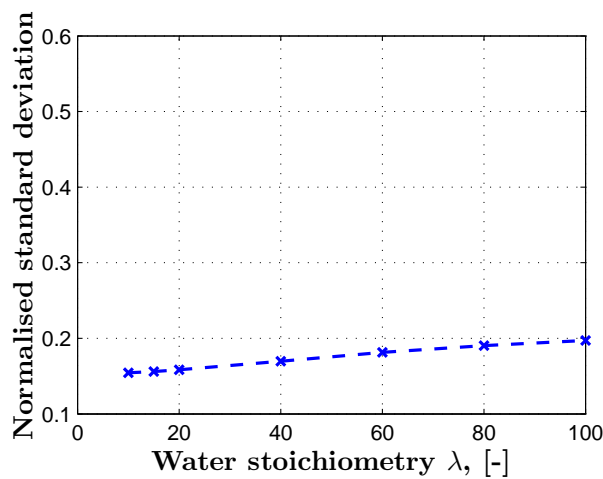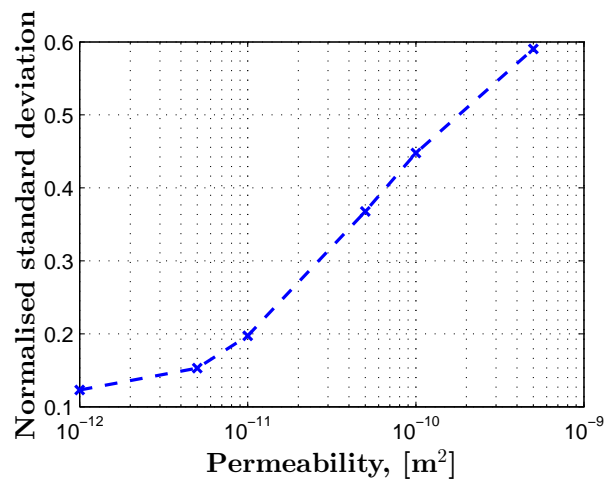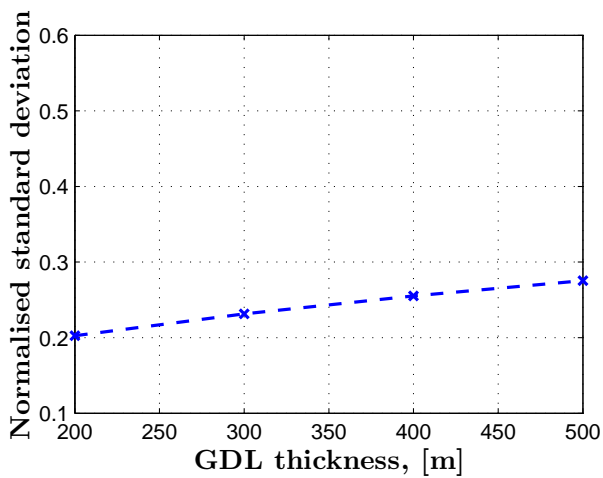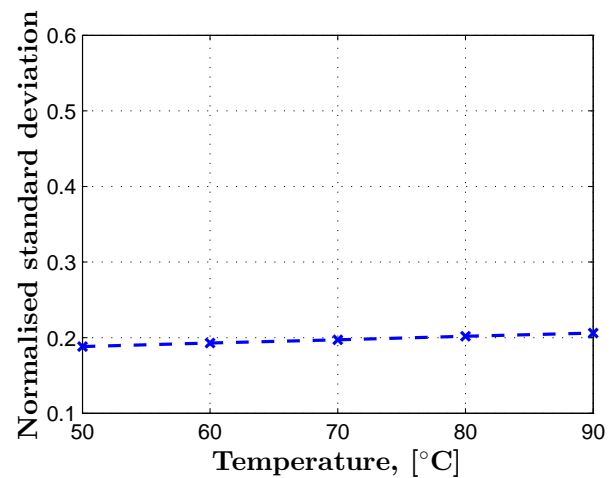
Figure 6: Channel mass flow standard deviation as a function of water stoichiometry (a), permeability (b), GDL thickness (c) and fluid temperature (d), respectively.

ity, a significant difference would not be expected as function of temperature. However, the increase that does occur with temperature may reflect some small inertial, or viscous affects due to the slightly increase volume flow in the channels.

CONCLUSION

In this work, the extent of flow maldistribution in an interdigitated, circular-planar anode flow field of a PEMEC was investigated using a macroscopic, steady-state, three-dimensional, single-phase, computational fluid dynamics model. It was found that an uneven mass flow distribution could be observed within the GDL. Moreover, a parametric study underlined that the extent of flow maldistribution,

shows a strong dependence on viscous permeability and weaker dependence on water stoichiometry, GDL thickness and temperature. Furthermore, it appears that the dependence on viscous permeability exhibits a threshold around $1.0 \cdot 10^{-11}$ m^2. Below this point, the dependence reduces rapidly and the porous domain dominates the flow maldistribution.

REFERENCES

[1] Carmo M, Fritz DL, Mergel J, Stolten D. *A comprehensive review on PEM water electrolysis*. International Journal of Hydrogen Energy, 38 (2013) 4901-4934.

[2] Zeng K, Zhang D. *Recent progress in alkaline water electrolysis for hydrogen production and applications*. Progress in Energy and Combustion Science 36 (2010) 307-326

[3] Pickard WF, Shen AQ, Hansing NJ. *Parking the power: strategies and physical limitations for bulk energy storage in supply-demand matching on a grid whose input power is provided by intermittent sources*. Renewable & Sustainable Energy Reviews, Oct 2009;13(8):1934-45

[4] Hedegaard K, Meibom P. *Wind power impacts and electricity storage e a time scale perspective*. Renewable Energy Jan 2012;37(1):318-24

[5] O'Hayre R, Cha SW, Whitney C, Fritz PB. *Fuel Cell Fundamentals*. John Wiley & Sons, Inc., ISBN 978-0-470-25843-9, 2009

[6] Gutierrez-Martin F, Guerrero-Hernandez I. *Balancing the grid loads by large scale integration of hydrogen technologies: the case of the Spanish power system*. International Journal of Hydrogen Energy, Jan 2012;37(2):1151-61.

[7] Berning T, Kær SK. 2012. *Low stoichiometry operation of a proton exchange membrane fuel cell employing the interdigitated flow field: A modeling study*. International Journal of Hydrogen Energy. 37(10):8477-8489

[8] Wang L, Liu H. *Performance studies of PEM fuel cells with interdigitated flow fields*. Journal of Power Sources 134 (2004) 185-196

[9] Wang XD, Duan YY, Yan WM, Weng FB. *Effect of humidity of reactants on the cell performance of PEM fuel cells with parallel and interdigitated flow field designs*. Journal of Power Sources 176 (2008) 247-258

[10] Li X, Sabir I. *Reviewof bipolar plates in PEM fuel cells: Flow-field designs*. International Journal of Hydrogen Energy 30 (2005) 359 - 371

[11] Ito H, Maeda T, Nakano A, Hasegawa Y, YokoiNb, Hwang CM, Ishida M, Kato A, Yoshida T. *Effect of flow regime of circulating water on a proton exchange membrane electrolyzer*. International Journal of Hydrogen Energy 35 (2010) 9550 - 9560

[12] Nie J, Chen Y. *Numerical modeling of three-dimensional two-phase gas-liquid flow in the flow field plate of a PEM electrolysis cell*. International Journal of Hydrogen Energy 35 (2010) 3183 - 3197

[13] Whitaker, S. *ADVANCES IN THEORY OF FLUID MOTION IN POROUS MEDIA*. Industrial & Engineering Chemistry 61 (1969) 14-28

[14] Slattery, JC. *Single-phase flow through porous media*. AIChE Journal 15 (1969) 866-872 year = 1969

[15] Tomadakis MM, Robertson TJ. *Viscous Permeability of Random Fiber Structures: Comparison of Electrical and Diffusional Estimates with Experimental and Analytical Results*. Journal of Composite Materials, 39(2), pp. 163-188. 2005

[16] Jakobsen, HA. *Chemical Reactor Modeling*. Springer Berlin Heidelberg, 2008, p. 335-501